Deformation of an elastic triangle in equilibrium under gravity

A. H. Opie
The School of Mathematics, The University of New South Wales, Kensington, New South Wales 2033, Australia

J. Grindlay
Guelph-Waterloo Programme for Graduate Work in Physics, Waterloo Campus, University of Waterloo, Waterloo, Ontario, Canada N2L 3G1

(Received 7 March 1994)

The equilibrium state of a triangular pile of particles interconnected by linear springs and subjected to the force of gravity is investigated numerically. The three strain components describing the deformation of the pile, the density change, and the supporting stress field are calculated. The results (a) exhibit an unexpected richness in behavior and (b) show evidence of a thermodynamic limit in small (~ 100 layers) piles.

PACS number(s): 46.10.+z, 01.55.+b

I. INTRODUCTION

The theoretical analysis of the equilibrium contact force distributions in piles of rigid disks and blocks [1–6] has been stimulated by the difficulty in interpreting the experimental results obtained from measurements on piles of sand and fertilizer [7]. In the simplest case, one attempts to calculate the forces acting in a triangular pile of smooth, rigid disks in equilibrium under gravity. Two unexpected results emerged from this algebraic analysis [5,6]. First of all, the force distribution (the set of all disk-disk forces) in a given geometrical distribution is not unique but depends on the way in which the pile is constructed. Second in the case of a symmetrically built pile, the maximum shearing force occurs not at the base under the apex, where one might have expected, but rather at the bottom two corners. In contrast, in the practical cases of piles of sand and fertilizer, the maximum shear stress occurs on the base roughly halfway between the center and the perimeter [7].

Given the unexpected force distributions seen both theoretically and experimentally in a rigid pile, we decided to explore the case of an elastic pile of particles, in equilibrium under gravity. We had two aims, one to calculate the deformation distribution within the pile and two to check for the existence of a thermodynamic limit [8] for the pile. If a model possesses a thermodynamic limit, then certain properties of the model are independent of the size of the system, provided the number of particles making up the model is sufficiently large. The elastic pile model described below is not homogeneous in the deformed state and so the standard thermodynamic limit proofs [8] do not apply. Similar remarks hold for the pile of rigid disks. (The contact force distribution is not homogeneous and the contact forces are not conservative.) As we shall describe below, a thermodynamic limit does exist for the elastic pile and evidence for this appears in small (~ 100 rows) piles.

Our model consists of a triangular pile of point particles interconnected by linear springs and subjected to gravity. The problem is to determine the shifts in equilibrium positions caused by the gravitational forces. Once we have these shifts, we can determine the gravity induced deformation of the triangle. A general algebraic solution for the equilibrium problem in an arbitrary large triangle proved to be elusive and so we carried out the numerical analysis, which we report below. As in the rigid disk case, the results were unexpected. The pattern of deformations, described by three strain tensor components, turns out to depend critically on the relative strengths of the springs used to link particles within rows and between rows in the triangle. These patterns are not at all what one would expect *a priori*. Our model provides another example of what appears to be a simple system exhibiting surprisingly complex behavior.

The triangular model and the equilibrium conditions are described in Sec. II. In Sec. III we reduce the problem to dimensionless form in preparation for computing. We also introduce a microscopically defined strain tensor and its dimensionless form. Sections IV–VIII contain descriptions of the numerical results for the three strain components, the mass density change, and the reaction forces supporting the weight of the triangle. Section IX contains a brief summary and the Appendix includes the definition of a microscopic strain tensor.

II. MODEL

Consider a regular, triangular array of particles of mass m connected by linear, unstretched springs as shown in Fig. 1. The springs connecting particles in adjacent rows have spring constant λ and unstretched length a; the corresponding parameters for the springs within rows are λ' and a'. Thus, the inner angle $\theta=\arccos(a'/2a)$, see Fig. 1. The N rows are labeled from the vertex down by $n=1,2,\ldots,N$; within each row the particles are labeled from the left $s=1,2,\ldots,n$, see Fig. 1. Within the array the (n,s)th particle is surrounded by six nearest neighbors, Fig. 2, and interacts via springs only with these particles. We introduce a set of

Cartesian axes with the origin at the apex; the Ox_1 axis is parallel to the rows and the Ox_2 is pointing away from the array, see Fig. 1. The position coordinates of the (n,s)th particle are then

$$x_1(n,s)=a\cos\theta(2s-n-1)\ ,$$
$$x_2(n,s)=a\sin\theta(1-n)\ . \tag{1}$$

This two-dimensional array of particles, connected by unstretched springs, is in static equilibrium. Now let us suppose that (a) gravity is switched on and acts in the negative Ox_2 direction and (b) the bottom layer of particles $n=N$ is supported to prevent any vertical motion. The new equilibrium position of the (n,s)th particle is denoted $\mathbf{x}(n,s)+\mathbf{u}(n,s)$. The shifts or displacements $\mathbf{u}(n,s)$ are solutions to the particle equilibrium conditions, containing both spring and gravitational forces.

It is a simple exercise to write down these equilibrium conditions; for the (n,s)th particle they are, in the Ox_1 direction,

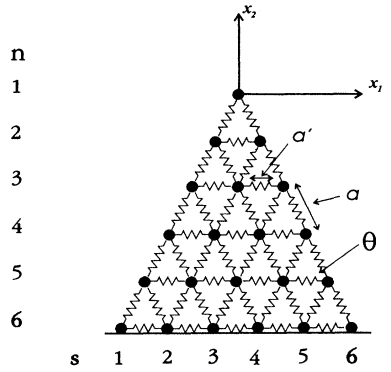

FIG. 1. Triangular array of particles and springs in equilibrium in the absence of gravity. The rows are labeled $n=1,2,\ldots,N$ and within the rows the particles are labeled $s=1,2,\ldots,n$. The bottom row, $n=N$ is in contact with a solid, smooth line.

$$\begin{aligned}0=&4\lambda'\cos^2\theta[u_1(n,s+1)-2u_1(n,s)+u_1(n,s-1)]\\&+\lambda\cos\theta\{[u_1(n-1,s)+u_1(n-1,s-1)+u_1(n+1,s)+u_1(n+1,s+1)-4u_1(n,s)]\cos\theta\\&\quad+[u_2(n-1,s)-u_2(n-1,s-1)+u_2(n+1,s)-u_2(n+1,s+1)]\sin\theta\}\end{aligned} \tag{2}$$

and in the Ox_2 direction,

$$\begin{aligned}0=&\lambda\sin\theta\{[u_1(n-1,s)-u_1(n-1,s-1)+u_1(n+1,s)-u_1(n+1,s+1)]\cos\theta\\&+[u_2(n-1,s)+u_2(n-1,s-1)+u_2(n+1,s)+u_2(n+1,s+1)-4u_2(n,s)]\sin\theta\}-w\ .\end{aligned} \tag{3}$$

$w=mg$ is the weight of an individual particle. The equivalent expressions for particles on the left edge are

$$\begin{aligned}0=&4\lambda'\cos^2\theta[u_1(n,2)-u_1(n,1)]\\&+\lambda\cos\theta\{[u_1(n-1,1)+u_1(n+1,1)+u_1(n+1,2)-3u_1(n,1)]\cos\theta\\&\quad+[u_2(n-1,1)+u_2(n+1,1)-u_2(n+1,2)-u_2(n,1)]\sin\theta\}\end{aligned} \tag{4}$$

and

$$\begin{aligned}0=&\lambda\sin\theta\{[u_1(n-1,1)+u_1(n+1,1)-u_1(n+1,2)-u_1(n,1)]\cos\theta\\&+[u_2(n-1,1)+u_2(n+1,1)+u_2(n+1,2)-3u_2(n,1)]\sin\theta\}-w\ .\end{aligned} \tag{5}$$

Analogous results hold on the right edge. The horizontal supporting line prevents any vertical shifts by the particles in the bottom layer, i.e.,

$$u_2(N,s)\equiv 0,\quad s=1,2,\ldots,N\ . \tag{6}$$

The equilibrium conditions in this bottom row then take the form

$$\begin{aligned}0=&4\lambda'\cos^2\theta[u_1(N,s+1)-2u_1(N,s)+u_1(N,s-1)]\\&+\lambda\cos\theta\{[u_1(N-1,s)+u_1(N-1,s-1)-2u_1(N,s)]\cos\theta+[u_2(N-1,s)-u_2(N-1,s-1)]\sin\theta\}\end{aligned} \tag{7}$$

and

$$\begin{aligned}0=&\lambda\sin\theta\{[u_1(N-1,s)-u_1(N-1,s-1)]\cos\theta\\&+[u_2(N-1,s)+u_2(N-1,s-1)]\sin\theta\}\\&-w+R(s)\ ,\end{aligned} \tag{8}$$

where $R(s)$ is the normal, reaction force acting on the sth particle in this row. We assume that the supporting line is smooth so that no horizontal clamping or frictional force appears in (7).

In a pyramid of N rows there are $N(N+1)/2$ particles and so $N(N+1)$ equilibrium conditions. The corresponding $N(N+1)$ unknowns are the $N(N+1)/2$ components $u_1(n,s)$, $n=1,2,\ldots,N$, $s=1,2,\ldots,n$; the $N(N-1)/2$ components $u_2(n,s)$, $n=1,2,\ldots,N-1$, $s=1,2,\ldots,n$; and the N forces $R(s)$, $s=1,2,\ldots,N$.

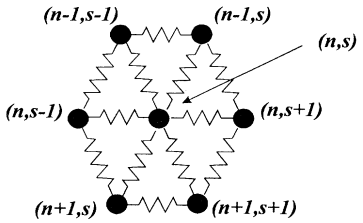

FIG. 2. Labeling of the six nearest neighbors of the (n,s)th interior particle.

Once we have obtained a solution to the equilibrium conditions, we can then determine the variation of strain through the pile. We have chosen to use the following microscopically derived strain tensor ϵ_{ij} (see Appendix):

$$\epsilon_{11}=[u_1(n,s+1)-u_1(n,s)]/2a\cos\theta\ , \tag{9}$$

$$\epsilon_{22}=[2u_2(n-1,s)-u_2(n,s)-u_2(n,s+1)]/2a\sin\theta\ , \tag{10}$$

$$\epsilon_{12}=\{2u_1(n-1,s)-u_1(n,s)-u_1(n,s+1)+\tan\theta \times[u_2(n,s+1)-u_2(n,s)]\}/4a\sin\theta\ . \tag{11}$$

The fractional change in mass density is (mass per unit area) $\Delta\rho/\rho=-(\epsilon_{11}+\epsilon_{22})$. With the choice of normal strains given in (9) and (10), we find

$$\Delta\rho/\rho=-\frac{1}{2a\sin\theta}\{2u_2(n-1,s)-u_2(n,s) -u_2(n,s+1)+\tan\theta \times[u_1(n-1,s)-u_1(n,s)]\}\ . \tag{12}$$

III. NUMERICAL SOLUTIONS

We shall now describe the results of a numerical analysis of the equilibrium states of the triangle described above. The first step is to choose dimensionless variables. The position coordinates x_i and displacements u_i are scaled in the following manner:

$$\tilde{x}_1(n,s)=x_1(n,s)/[Na\cos\theta]\ , \tag{13}$$

$$\tilde{x}_2(n,s)=x_2(n,s)/[Na\sin\theta]\ , \tag{14}$$

$$\tilde{u}_1(n,s)=u_1(n,s)\frac{\lambda}{w}\sin\theta\cos\theta\ , \tag{15}$$

$$\tilde{u}_2(n,s)=u_2(n,s)\frac{\lambda}{w}\sin^2\theta\ . \tag{16}$$

In these dimensionless coordinates [Eqs. (13) and (14)] the peak of the triangle is at (0,0) and the two lower corners are at $(\pm1,-1)$. The (n,s)th equilibrium conditions for these new displacements [Eqs. (15) and (16)] take the simple one-parameter form

$$0=\gamma[\tilde{u}_1(n,s+1)-2\tilde{u}_1(n,s)+\tilde{u}_1(n,s-1)] +[\tilde{u}_1(n-1,s)+\tilde{u}_1(n-1,s-1)+\tilde{u}_1(n+1,s)+\tilde{u}_1(n+1,s+1)-4\tilde{u}_1(n,s)] +[\tilde{u}_2(n-1,s)-\tilde{u}_2(n-1,s-1)+\tilde{u}_2(n+1,s)-\tilde{u}_2(n+1,s+1)]\ , \tag{17}$$

$$0=[\tilde{u}_1(n-1,s)-\tilde{u}_1(n-1,s-1)+\tilde{u}_1(n+1,s)-\tilde{u}_1(n+1,s+1)] +[\tilde{u}_2(n-1,s)+\tilde{u}_2(n-1,s-1)+\tilde{u}_2(n+1,s)+\tilde{u}_2(n+1,s+1)-4\tilde{u}_2(n,s)]-1\ , \tag{18}$$

where

$$\gamma=4\lambda'/\lambda\ . \tag{19}$$

For the special case of identical springs, $\lambda'=\lambda$, $\gamma=4$, and $\theta=\pi/3$.

Along the left edge,

$$0=\gamma[\tilde{u}_1(n,2)-\tilde{u}_1(n,1)]+[\tilde{u}_1(n-1,1)+\tilde{u}_1(n+1,1)+\tilde{u}_1(n+1,2)-3\tilde{u}_1(n,1) +\tilde{u}_2(n-1,1)+\tilde{u}_2(n+1,1)-\tilde{u}_2(n+1,2)-\tilde{u}_2(n,1)]\ , \tag{20}$$

and

$$0=\tilde{u}_1(n-1,1)+\tilde{u}_1(n+1,1)-\tilde{u}_1(n+1,2)-\tilde{u}_1(n,1) +\tilde{u}_2(n-1,1)+\tilde{u}_2(n+1,1) +\tilde{u}_2(n+1,2)-3\tilde{u}_2(n,1)-1\ . \tag{21}$$

Since the triangle-support contact is assumed to be smooth, the equilibrium conditions in the bottom row yield an equation for the displacements

$$0=\gamma[\tilde{u}_1(N,s+1)-2\tilde{u}_1(N,s)+\tilde{u}_1(N,s-1)] +[\tilde{u}_1(n-1,s)+\tilde{u}_1(N-1,s-1)-2\tilde{u}_1(N,s) +\tilde{u}_2(N-1,s)-\tilde{u}_2(N-1,s-1)] \tag{22}$$

and an equation for the normal reactions

$$R(s)=w[1-\tilde{u}_1(N-1,s)+\tilde{u}_1(N-1,s-1) +\tilde{u}_2(N-1,s)+\tilde{u}_2(N-1,s-1)]\ . \tag{23}$$

We note that the shifts $\tilde{u}_1(n,s)$, $\tilde{u}_2(n,s)$, and the ratio

$R(s)/w$ are functions of two parameters, namely N and γ and are independent of the angle θ.

Substituting for the displacements in terms of the tilde quantities in the expressions for the strains (9), (10), and (11), and fractional change in mass density (12) we find that

$$\epsilon_{11}=\left[\frac{mg}{2\lambda a}\frac{1}{\sin\theta\cos^2\theta}\right]\tilde{\epsilon}_{11}\ , \tag{24}$$

$$\epsilon_{12}=\left[\frac{mg}{4\lambda a}\frac{1}{\cos\theta\sin^2\theta}\right]\tilde{\epsilon}_{12}\ , \tag{25}$$

$$\epsilon_{22}=\left[\frac{mg}{2\lambda a}\frac{1}{\sin^3\theta}\right]\tilde{\epsilon}_{22}\ , \tag{26}$$

$$\Delta\sigma/\sigma=\left[\frac{mg}{2\lambda a}\frac{1}{\sin^3\theta}\right]\overline{\Delta\sigma/\sigma}\ , \tag{27}$$

where the tilde quantities are

$$\tilde{\epsilon}_{11}[\tilde{u}_1(n,s+1)-\tilde{u}_1(n,s)]\ , \tag{28}$$

$$\tilde{\epsilon}_{12}=[\tilde{u}_2(n,s+1)-\tilde{u}_2(n,s)+2\tilde{u}_2(n,s-1) -\tilde{u}_1(n,s)-\tilde{u}_1(n,s+1)]\ , \tag{29}$$

$$\tilde{\epsilon}_{22}=[2\tilde{u}_2(n,s-1)-\tilde{u}_2(n,s)-\tilde{u}_2(n,s+1)]\ , \tag{30}$$

and

$$\overline{\Delta\sigma/\sigma}=-[\tilde{\epsilon}_{22}+\tan^2\theta\tilde{\epsilon}_{11}]\ . \tag{31}$$

Each of the new scaled strains, (28), (29), and (30), is expressible in terms of the tilde displacements alone and hence are functions only of the model parameter N and γ. In contrast, the scale mass density change, (31), is a function of N, γ, and the inner angle θ.

A FORTRAN program was written to seek solutions iteratively to the equilibrium conditions for given values of N and the parameter γ. We use the Gauss-Seidel over-relaxation method with relaxation parameter equal to 1.85 [9]. In this method, one guesses at the solution to the equilibrium conditions and the algorithm then homes into the correct solution. This method works only if the system is locally stable. In all the various solutions we sought for different model parameters, we saw no evidence of instability, even when we tried initial guesses, which were not symmetric about the vertical axis through the apex of the triangle.

Consider first the scaled strain $\tilde{\epsilon}_{11}$, (28). We ran our program to determine the function, $\tilde{\epsilon}_{11}(\tilde{x}_1,\tilde{x}_2)$, for fixed γ and a variety of N values. This normal strain field changed appreciably with increasing N—as one might expect in a pile of increasing size. However, the normalized strain field $\tilde{\epsilon}_{11}(\tilde{x}_1,\tilde{x}_2)/\tilde{\epsilon}_{11}^{\max}$, where $\tilde{\epsilon}_{11}^{\max}$ is the maximum of $|\tilde{\epsilon}_{11}(\tilde{x}_1,\tilde{x}_2)|$, proved to be much less sensitive to changes in N and indeed tended to a limit independent of N as the pile size was increased. For example, in the case of $\gamma=4$, as N was increased from $N=80$ to $N=100$ the field $\tilde{\epsilon}_{11}(\tilde{x}_1,\tilde{x}_2)/\tilde{\epsilon}_{11}^{\max}$ changed by less than 1%. Similar results were found for other γ values. Note that $\epsilon_{11}(\tilde{x}_1,\tilde{x}_2)/\epsilon_{11}^{\max}=\tilde{\epsilon}_{11}(\tilde{x}_1,\tilde{x}_2)/\tilde{\epsilon}_{11}^{\max}$, (24), and so the same conclusions hold for the strain field, $\epsilon_{11}(\tilde{x}_1,\tilde{x}_2)$. The other strains, (29) and (30), and the mass density change, (31), exhibited a similar pattern of behavior.

These results show that (a) a thermodynamic limit exists for the strain and mass density change fields scaled to their maxima and regarded as functions of the position coordinates scaled to the dimensions of the triangle and (b) the system approaches to within 1% of this limit for $N\sim 100$.

We note that the displacement component u_2 and the normal strains ϵ_{11} and ϵ_{22} are even functions under reflection in the vertical axis of the triangle, $x_1\rightarrow -x_1$; in contrast u_1 and the shear strain ϵ_{12} are odd functions under reflection.

IV. NORMAL STRAIN ϵ_{11}

Figure 3(a) contains a contour plot of $\tilde{\epsilon}_{11}/\tilde{\epsilon}_{11}^{\max}$ for $\gamma=4$, where $\tilde{\epsilon}_{11}$ is the scaled normal strain [Eq. (28)] and $\tilde{\epsilon}_{11}^{\max}$ is the maximum value of $\tilde{\epsilon}_{11}$ occurring within the triangle. The vertical and horizontal axes represent the scaled coordinates $\tilde{x}_2$ and $\tilde{x}_1$ [Eqs. (13) and (14)]. Because of the symmetry properties of the strains under reflection in the vertical axis, we show only the contours on the right side of the triangle. As noted above, $\tilde{\epsilon}_{11}$ and $\tilde{\epsilon}_{11}^{\max}$ are scaled by the same quantity [Eq. (24)] and so the contour plot also describes the ratio $\epsilon_{11}/\epsilon_{11}^{\max}$.

The strain ϵ_{11} displays both positive and negative values within the triangle; it is positive for $\tilde{x}_2<-0.25$ and $\tilde{x}_2>-0.05$, and negative in the intervening region, see hatched area in Fig. 3(a). The largest magnitude $\epsilon_{11}=\epsilon_{11}^{\max}$ occurs at the base vertically below the apex; in the tilde coordinate system, this is the point $(0,-1)$. The smallest negative strain is $-0.0071\epsilon_{11}^{\max}$ and this occurs at $(0,-0.2)$. Within the two positive strain regions, the horizontal displacement components $\tilde{u}_1(n,s)$ are all positive in the right half of the triangle, i.e., the equilibrium positions move horizontally away from the vertical axis of the triangle; within the negative strain regions, the horizontal displacement components are negative, (displacements towards the vertical axis). However in the boundary region $\tilde{x}_2\sim -0.25$ we find examples of particles with negative strains $\epsilon_{11}<0$, and positive displacements $u_1(n,s)>0$.

For large values of γ, the negative strain region disappears and ϵ_{11} drops off more rapidly from the maximum at the base.

As the ratio γ is reduced from the value 4, the minimum strain at the peak decreases and other two regions of negative strain develop at the lower corners. For the case shown in Fig. 3(b), $\gamma=0.4$, the minimum near the peak is $\epsilon_{11}=-0.112\epsilon_{11}^{\max}$ at $(0,-0.14)$. The minima at the lower corners have the value $\epsilon_{11}=-0.038\epsilon_{11}^{\max}$ and occur at $(\pm 0.96,-1)$.

V. NORMAL STRAIN ϵ_{22}

For values of $\gamma=4.0$ and above, the normal strain ϵ_{22} is negative everywhere in the triangle with a maximum magnitude $\epsilon_{22}^{\max}$ occurring at the center of the base, coor-

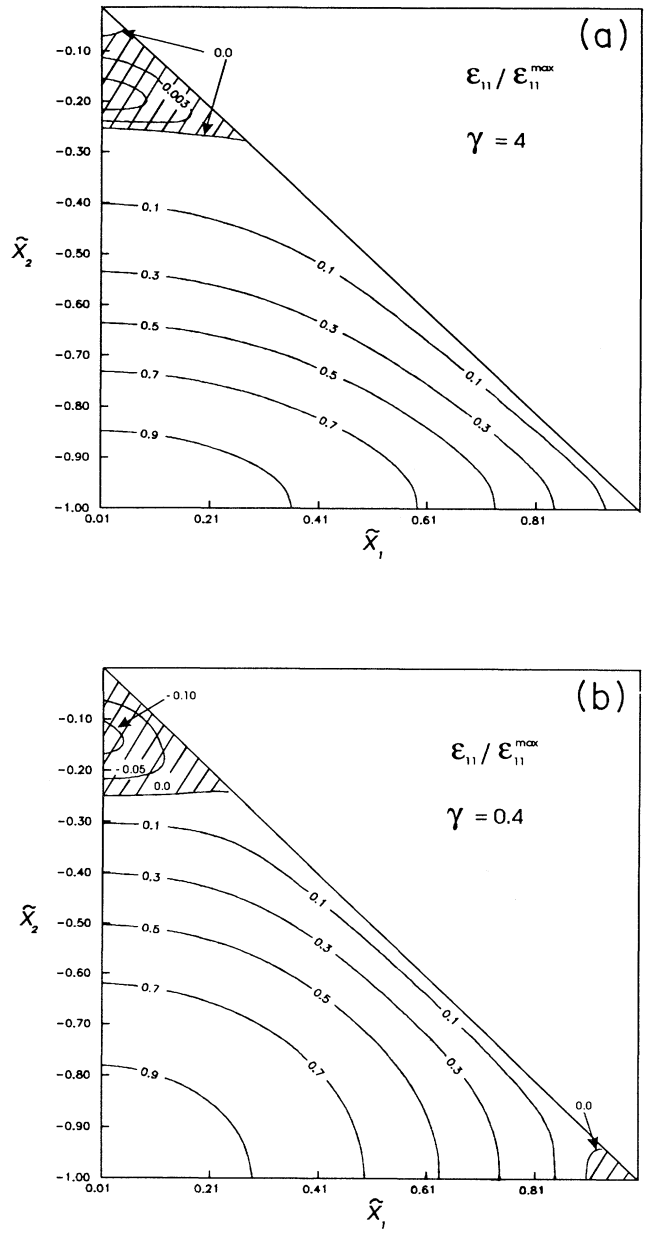

FIG. 3. Contour plot of the normal strain ϵ_{11} normalized to the maximum value ϵ_{11}^{max} for the two cases (a) $\gamma=4$ and (b) $\gamma=0.4$. The position of points within the triangle are shown using the normalized coordinates $\tilde{x}_1$ and $\tilde{x}_2$ [Eqs. (13) and (14)]. The negative strain regions are shown crossed hatched. The data in these and the following seven contour plots were obtained for a pile with 100 rows.

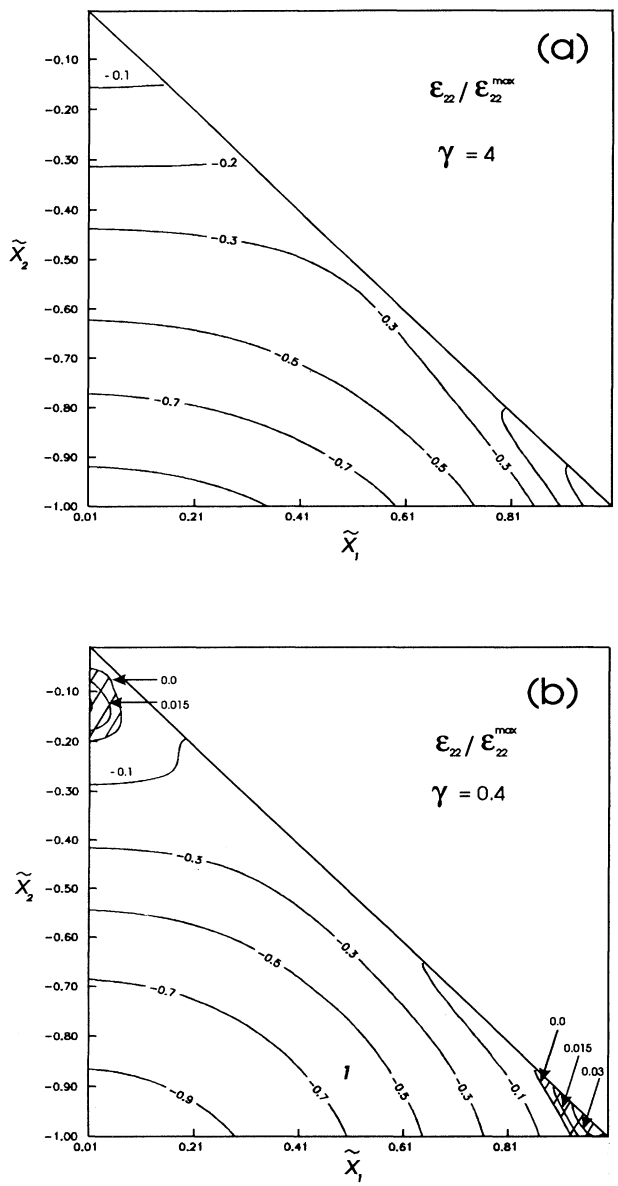

FIG. 4. Contour plot of the normal strain ϵ_{22} normalized to the maximum magnitude ϵ_{22}^{max} for the two cases (a) $\gamma=4$ and (b) $\gamma=0.4$.

dinates $(0,-1)$. Figure 4(a) contains the contour maps of $\epsilon_{22}/\epsilon_{22}^{max}$ for the value $\gamma=4$. For smaller spring constant ratios, regions of positive strain appear at the peak and lower two corners: see the hatched regions in Fig. 4(b) for the case $\gamma=0.4$. There are three positive maxima; one near the peak $(0,-0.14)$ with $\epsilon_{22}=0.034\epsilon_{22}^{max}$, and the two near the lower corners $(\pm 0.94,-0.97)$ with $\epsilon_{22}=0.040\epsilon_{22}^{max}$.

VI. SHEAR STRAIN ϵ_{12}

Since the shear strain is an odd function under reflection in the vertical axis, $\tilde{x}_1=0$ is a line of vanishing strain, $\epsilon_{12}\equiv 0$. For values of $\gamma=4$ and above, the shear strain ϵ_{12} is positive (negative) everywhere to the right (left) of the vertical axis. The case of $\gamma=4$ is shown in Fig. 5(a). From this figure, we see that $|\epsilon_{12}|$ reaches a maximum magnitude on the sloping boundary at the points $(\pm 0.54,-0.54)$.

As γ is reduced in from the value 4, the shear strain exhibits both positive and negative values in both halves. The case of $\gamma=0.4$ is shown in Fig. 5(b). In the right half

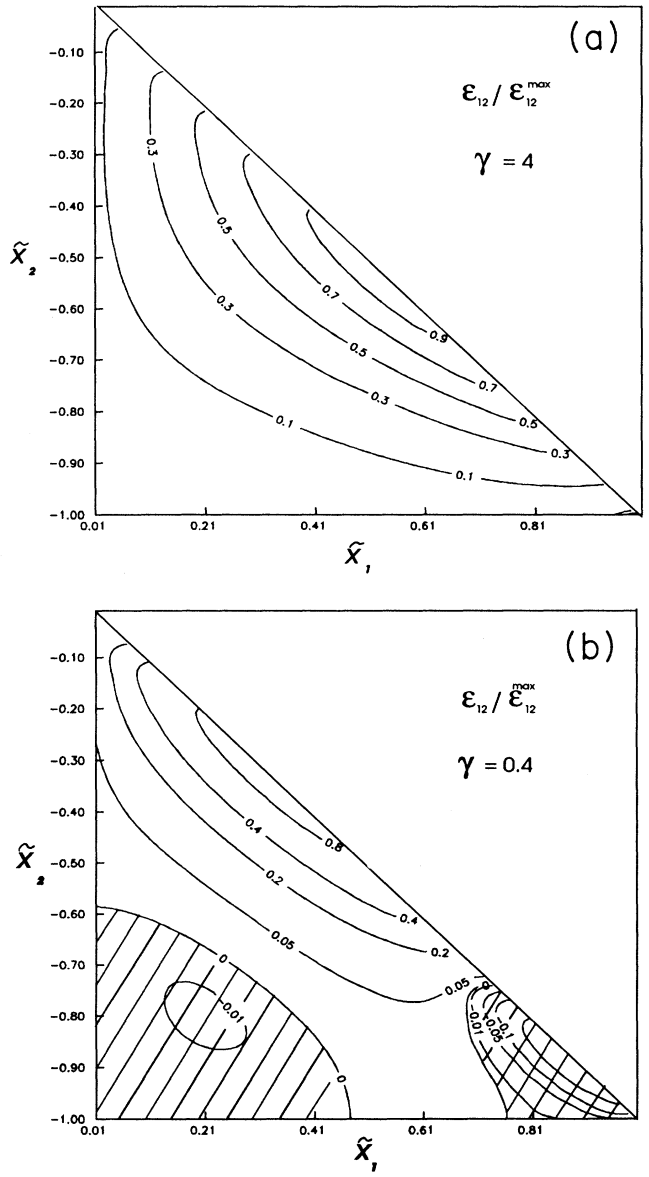

FIG. 5. Contour plot of the shear strain ϵ_{12} normalized to the maximum value ϵ_{12}^{max} for the two cases (a) $\gamma=4$ and (b) $\gamma=0.4$.

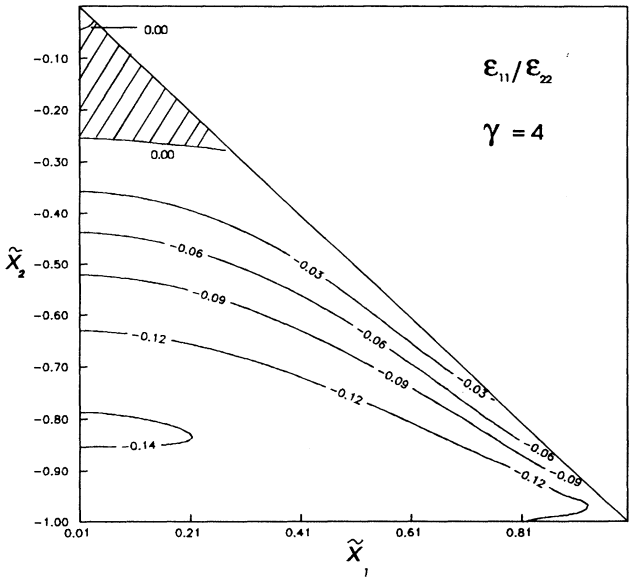

FIG. 6. Contour plot of the ratio of normalized strains $\tilde{\epsilon}_{11}/\tilde{\epsilon}_{22}$ for the case $\gamma=4$. The hatched areas are regions of positive values.

of the triangle there is a maximum ϵ_{12}^{max} at $(0.33,-0.33)$ on the boundary and two minima, one $\epsilon_{12}=-0.35\epsilon_{12}^{max}$ at $(0.91,-0.91)$ and the other $\epsilon_{12}=-0.012\epsilon_{12}^{max}$ at $(0.22,-0.80)$.

VII. FRACTIONAL DENSITY CHANGE $\Delta\rho/\rho$

The density change $\Delta\rho/\rho$ is a linear combination of $\tilde{\epsilon}_{11}$ and $\tilde{\epsilon}_{22}$ [Eqs. (27) and (31)]. For a given triangle and hence given angle θ, lines of vanishing density change occur at points for which

$$\tilde{\epsilon}_{11}/\tilde{\epsilon}_{22}=-\cot^2\theta\ . \tag{32}$$

In Fig. 6 we show contour plots of the ratio $\tilde{\epsilon}_{11}/\tilde{\epsilon}_{22}$ for $\gamma=4$. Since $\tilde{\epsilon}_{22}$ is negative everywhere, see Sec. III above, the ratio $\tilde{\epsilon}_{11}/\tilde{\epsilon}_{22}$ is negative only where $\tilde{\epsilon}_{11}$ is positive, i.e., in a small region at the peak and below approximately the line $\tilde{x}_2=-0.25$, see Sec. III above. The maximum magnitude of $\tilde{\epsilon}_{11}/\tilde{\epsilon}_{22}$ occurs at $(0,-0.82)$ and has a value 0.141. Thus, for the case $\gamma=4$, the fractional change $\Delta\rho/\rho$ will vanish (and hence change sign) for triangles with $\theta>\arctan[\sqrt{1/0.141}]=20.6°$. As an example we have constructed the graph of the contours of the fractional density charge for $\gamma=4$ and $\theta=\arctan(10/3)$, Fig. 7(a). We see here that the contour $\Delta\rho/\rho=0$ coincides with the contour $\tilde{\epsilon}_{11}/\tilde{\epsilon}_{22}=-0.09$ in Fig. 6. Above (below) this contour, Fig. 7(a), the effect of gravity is to increase (decrease) the density.

For smaller values of γ, the normal strain $\tilde{\epsilon}_{22}$ vanishes along certain contours, see Sec. V above, and so $\tilde{\epsilon}_{11}/\tilde{\epsilon}_{22}$ possess lines of singularities. The fractional density change contour graph for $\gamma=0.4$ and $\theta=\arctan\sqrt{(5/3)}=52.2°$ is shown in Fig. 7(b). The density change has two maxima, each of value $(\Delta\rho/\rho)^{max}$ say, at $(\pm0.32,-0.32)$. There is a local maximum $(\Delta\rho/\rho)=0.87(\Delta\rho/\rho)^{max}$ at $(0,-1)$. Minima occur at $(\pm0.89,-0.89)$ with $(\Delta\rho/\rho)=-0.33(\Delta\rho/\rho)^{max}$ and at $(0,-0.58)$ with $(\Delta\rho/\rho)=-0.041(\Delta\rho/\rho)^{max}$. The complex behavior seen here is a consequence of the pattern of zeros in $\tilde{\epsilon}_{11}$ and $\tilde{\epsilon}_{22}$, Figs. 3(b) and 4(b).

VIII. REACTION $R(s)$

The reaction $R(s)$ of the supporting line on the sth particle is determined by the displacement components [Eq. (23)]. Given the displacement components $\tilde{u}_1$ and $\tilde{u}_2$, it is then a simple matter to calculate the ratio $R(s)/w$. Setting the total weight of the triangle

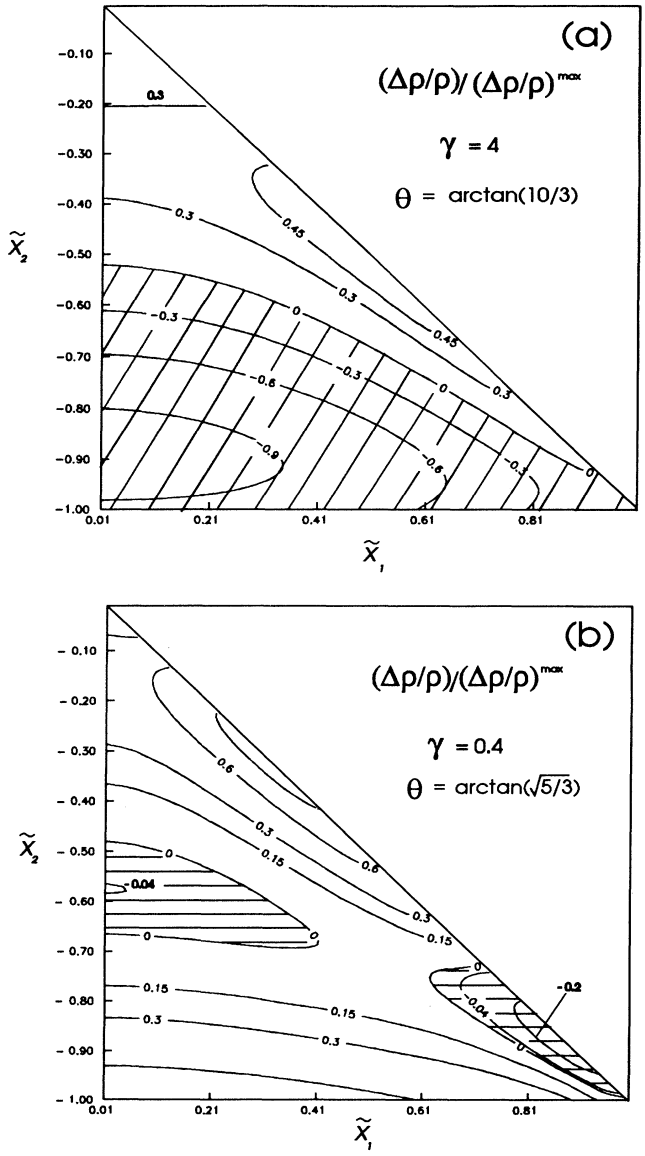

FIG. 7. Contour plot of the density change $(\Delta\rho/\rho)$ normalized to the maximum magnitude $(\Delta\rho/\rho)^{max}$ for the two cases (a) $\gamma=4$, $\theta=73.3°$ and (b) $\gamma=0.4$, $\theta=52.2°$. The hatched areas are regions of rarefaction.

$N(N+1)w/2=W$, we have plotted the ratio $R(s)/W$ in Fig. 8 for the three values $\gamma=40$, 4, and 0.4. As we see from these graphs, the reaction forces vary across the base of the triangle reaching a maximum under the apex and this maximum increases with decreasing γ.

There is no hint that by varying the spring constant ratio we could cause this maximum to move away from the point under the apex. This suggests that the solution to the problem of modeling the experimental results of Smid and Novosad [7] will not be found by introducing elastic disks.

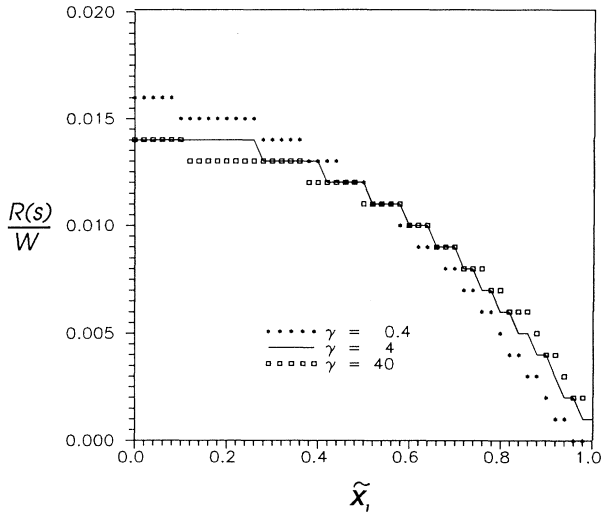

FIG. 8. Graph of the ratio of the normal reaction R [Eq. (23)], to the total weight W of the triangle vs the normalized coordinate $\tilde{x}_1$ for the three cases $\gamma=0.4$, 4, and 40, each with $N=100$.

IX. SUMMARY

We have carried out a numerical analysis of the equilibrium state of a triangular pile of particles interconnected by linear springs and subjected to the force of gravity. The results (a) show a complex pattern of strain and mass density behavior and (b) prove that this system approaches a thermodynamic limit for the case of small (~ 100 layers) piles.

APPENDIX: MICROSCOPIC STRAIN

The gravity induced deformation of the triangular array is described by the set of displacement components, $u_i(n,s)$, $i=1,2$, $n=1,\ldots,N$, and $s=1,\ldots,n$. To define the deformation gradient at the microscopic or atomic level, we proceed as follows. Let a particle initially at a point x_i be moved to a point $x_i+\delta x_i$. The deformation gradient tensor u_{ij} is defined as the set of quantities that relate the shift δx_i to the original position x_i in the form

$$\delta x_i=\sum_{j=1}^{2} u_{ji}x_j, \quad i=1,2 . \tag{A1}$$

To obtain expressions for the displacement gradients in the case of the triangular array described above, we choose to relate the positions and shifts of the $(n,s+1)$th and $(n-1,s)$th particles relative to the (n,s)th particle (see Fig. 2). Hence,

$$u_1(n,s+1)-u_1(n,s)=u_{11}2a\cos\theta , \tag{A2}$$

$$u_2(n,s+1)-u_2(n,s)=u_{12}2a\cos\theta , \tag{A3}$$

$$u_1(n-1,s)-u_1(n,s)=u_{11}a\cos\theta+u_{21}a\sin\theta , \tag{A4}$$

$$u_2(n-1,s)-u_2(n,s)=u_{12}a\cos\theta+u_{22}a\sin\theta . \tag{A5}$$

Solving for the displacement gradients from these four equations and substituting the results into the expressions for the infinitesimal strain tensor, we find that

$$\epsilon_{11}=u_{11}=[u_1(n,s+1)-u_1(n,s)]/2a\ \cos\theta\ , \tag{A6}$$

$$\epsilon_{22}=u_{22}=[2u_2(n-1,s) -u_2(n,s)-u_2(n,s+1)]/2a\ \sin\theta\ , \tag{A7}$$

$$\epsilon_{12}=(u_{12}+u_{21})/2 =\{2u_1(n-1,s)-u_1(n,s)-u_1(n,s+1) -\tan\theta[u_2(n,s)-u_2(n,s+1)]\}/4a\ \sin\theta\ . \tag{A8}$$

Strain is normally used to describe the deformation in continua and so we can think of the expressions (A6), (A7), and (A8) based on particle displacements, as microscopic strains, in the sense of strains defined at the microscopic level. We shall associate these strains with the (n,s)th particle. Clearly we can obtain different expressions for the microscopic strains by calculating the deformation gradient from the displacements of other sets of particles around the (n,s)th particle. However, in macroscopically sized bodies the variation among different definitions of microscopic strain will be negligible.

ACKNOWLEDGMENTS

This work was supported by the Natural Sciences and Engineering Council of Canada and the Australian Government.

[1] D. F. Bagster and R. Kirk, J. Powder Bulk Solids Technol. **9**, 19 (1985).
[2] E. Li and Bagster, Powder Technol. **63**, 277 (1990).
[3] K. Liffman, D. Y. C. Chan, and B. D. Hughes, Powder Technol. **42**, 255 (1992).
[4] D. C. Hong, Phys. Rev. E **47**, 760 (1993).
[5] J. Grindlay, Am. J. Phys. **61**, 469 (1993).
[6] J. Grindlay and A. H. Opie, preceding paper, Phys. Rev. E **51**, 718 (1995).
[7] J. Smid and J. Novosad, *Particle Technology,* (ICHE Symp. Series No. 3) (Institute of Chemical Engineers, Rugby, England, 1981).
[8] Thermodynamic limit theorems have been proved for homogeneous systems and certain classes of interatomic potentials. See, A. Munster, *Statistical Thermodynamics* (Springer, New York, 1969), Vol. 1.
[9] W. H. Press, B. P. Flannery, S. A. Teukolsky, and W. T. Vetterling, *Numerical Recipes* (Cambridge University, Cambridge, England, 1987).